THE ASTROPHYSICAL JOURNAL, 333:673–688, 1988 October 15

A MODEL FOR THE EFFECTS OF DUST ON THE SPECTRA OF DISK GALAXIES. I. GENERAL TREATMENT

GUSTAVO BRUZUAL A., GLADIS MAGRIS C., AND NURIA CALVET
Centro de Investigaciones de Astronomia, Mérida, Venezuela
Received 1986 July 7; accepted 1988 March 22

ABSTRACT

The radiative transfer equation is solved for a mixture of stars and dust grains distributed homogeneously in an infinite plane-parallel configuration. The effects of absorption and multiple scattering of light due to dust grains with the same optical properties as the interstellar dust in the Galaxy and in the LMC are evaluated and compared. The values of the albedo and the asymmetry parameter published in the literature allow us to solve the problem in the range from 1200 to 18,000 Å, with a resolution in wavelength of ~ 100 Å. The results are presented in the form of correction terms as a function of wavelength, inclination angle, and optical depth, τ, of the system. These terms can be used to correct the spectrum of a mixture of stars and dust to obtain the spectrum of the stellar component alone, or to introduce reddening into a synthetic galaxy spectrum. For small optical depths ($\tau < 1$) the correction terms depend critically on the inclination angle. The surface brightness profiles of spiral galaxies do not show this dependence, which implies that for these galaxies the optical depth is large ($\tau > 1$). We compute magnitudes and colors as a function of redshift for galaxies seen at different inclination angles and with different values of the optical depth through the plane of the galaxy. The difference between our correction terms and a straightforward application of the standard galactic reddening law is large, especially in the UV region of the spectrum. The correction terms should be preferred over the standard reddening law to take into account the effects of dust in the photometric properties of galaxies.

Subject headings: galaxies: photometry — interstellar: grains — interstellar: matter — radiative transfer

I. INTRODUCTION

The solution to the problem of radiative transfer in a dusty galaxy is of fundamental importance for the interpretation of faint galaxy spectral energy distributions (SEDs), magnitudes, colors, number counts, as well as color and redshift distributions at a given apparent magnitude. Detailed models that include the spectral evolution of galaxies (Bruzual and Kron 1980; Tinsley 1980; Koo 1981) have been partially successful in explaining the observed counts and color distributions of galaxies. None of these models includes the effects of dust in the model galaxies.

Dust clouds are prominent features in spiral and irregular galaxies, and $\sim 40\%$ of ellipticals show evidence of dust lanes (Sadler and Gerhard 1985). From our perspective in the Galaxy we know that starlight is reddened by dust grains when it travels through the interstellar medium. Scattering and absorption by dust grains remove preferentially blue photons from the light beam, producing a characteristic and predictable redness in the SED of the source, such that the color excess is correlated with the total extinction. The properties of dust grains found toward different directions in the Galaxy are uniform enough that an average reddening law (e.g., Seaton 1979) based on empirical data can be used satisfactorily to deredden stellar SEDs.

The scheme outlined above is applicable only when the dusty region is located between the source and the observer, as is the case for galactic stars. When we observe an external galaxy the situation is different. The reddening law can be used to correct the external galaxy SED from the effect of local dust along the line of sight to this galaxy. However, the effect on the galaxy SED of its own dusty regions cannot be accounted for in this manner. The path length traveled by light inside the external galaxy is so large that there is a nonnegligible probability that a photon scattered out of the beam is scattered again into the beam, or replaced by a different photon of the same wavelength. Similarly, photons that were traveling to start with in directions out of the line of sight to this galaxy may end up along this line after one or more scattering events. If the scattering process were wavelength independent, and given a sufficiently large optical depth through the external galaxy, we would expect that at all wavelengths as many photons were removed out of the beam as into the beam, producing no reddening in the observed SED. However, the probability that a photon be scattered rather than absorbed does depend on the photon wavelength and is measured by the albedo a_λ of the grains (Lillie and Witt 1976). The behavior of a_λ in the UV, which is the relevant spectral region at the faint light levels used in cosmological applications, is very different from that in the visible region. At those wavelengths at which a_λ is low, absorption occurs with higher probability than scattering. The absorbed photons heat the dust grains and this energy is reradiated at IR wavelengths. In addition, the angle dependence of the scattering process is also a function of the wavelength of the incoming photon. For instance, the Henyey and Greenstein (1941) asymmetry factor g_λ, which measures the average of the cosine of the scattering angle, is a function of wavelength.

A priori one might think that the effect of dust is only to redden the light coming out of galaxies and conclude that in the mixture of galaxies used in the models of Bruzual and Kron (1980), Tinsley (1980), and Koo (1981) red galaxies are artificially overrepresented. One might expect that mixtures of galaxies with a higher fraction of intrinsically blue galaxies would reproduce the observations equally well when the effects of dust and galaxy inclination are accounted for properly, at least in a statistical form. Before this presumption can be sustained one has to solve the radiative transfer equation in detail. In this equation the scattering and absorption processes are treated statistically and their effects introduced by means of a_λ and g_λ.

Different authors have considered this problem previously from different points of view. Holmberg (1975) introduced the cosecant law, which is applicable only for low values of the albedo and the optical depth (see below). For most galaxies this approximation is good enough in the visible region but fails in the UV. Elmegreen (1980) considered specific dust complexes in some bright external galaxies and solved the radiative transfer equation using an analytical approach. She considered only the wavelengths at which observations were available. In each case the geometry was chosen to match that of the complexes under study. Roberge (1983) presented an elegant analytical solution by means of the spherical harmonics method and applied it to H_2 band emission in molecular clouds, as well as to IR line emission from shocked molecular clouds. Mathis (1983) solved the radiative transfer problem using a numerical algorithm for optical and IR wavelengths of interest in the study of ionized nebulae.

None of these solutions is general enough to be used for our purpose of studying reddening effects in galaxies seen at different cosmological epochs. We need a recipe that can be used either to deredden observed galaxy SED or to introduce reddening into a synthetic galaxy SED, for any value of the reshift and the inclination of the galaxy.

In this paper we present a numerical solution to the radiative transfer problem in a mixture of stars and dust grains distributed homogeneously in an infinite plane-parallel configuration. The effects of absorption and multiple scattering of light due to dust grains with the same optical properties as the interstellar dust in the Galaxy are included. The values of a_λ and g_λ published in the literature allow us to solve the problem in the range from 1200 to 18,000 Å. The results are presented in the form of correction terms as a function of wavelength, inclination angle, and optical depth of the system. The correction terms are computed with enough resolution in wavelength (roughly every 100 Å) to correct galaxy spectra with the desired accuracy.

Section II contains the formulation of the radiative transfer problem in the case of interest and a description of the numerical technique used to integrate the transfer equation. In § III we present general results and discuss the uncertainties introduced into the correction factors by the observational uncertainties in a_λ, in g_λ, and in the extinction law. In § IV we use our correction terms to study the effects of reddening in the photometric properties of galaxies as a function of inclination angle, optical depth, and cosmological redshift. The conclusions are presented in § V.

II. THE MODEL

a) Formulation of the Problem

We solve the problem of radiative transfer inside a plane-parallel slab in which stars and dust grains are uniformly distributed. Because we neglect the presence of gas in this medium, starlight suffers absorption and scattering by dust grains only. The specific intensity of radiation, $I_\lambda(z, \mu)$, is a solution to the following equation of transfer, in which the intrinsic dust emissivity has been neglected,

$$\mu\, \partial I_\lambda(z, \mu)/\partial z = -\chi_\lambda I_\lambda(z, \mu) + \eta_\lambda^*(z, \mu) + \eta_\lambda^s(z, \mu) . \quad (1)$$

The dust thermal emission, which is most significant in the IR, is not included because we are interested mainly in the radiation emerging from the slab in the visible and UV regions of the spectrum. The independent variables in (1) are the depth z of the slab, measured along the direction perpendicular to the plane, and the angle $\theta = \cos^{-1} \mu$ between this direction and the direction of the light beam. χ_λ is the absorption coefficient of the medium at wavelength λ, $\eta_\lambda^*(z, \mu)$ is the emissivity of the stellar sources,

$$\eta_\lambda^s(z, \mu) = \chi_\lambda(a_\lambda/4\pi) \int I_\lambda(z, \mu')\Phi_\lambda(\Theta)d\Omega' , \quad (2)$$

is the contribution to the emissivity due to scattering by dust particles, where a_λ is the dust albedo, defined as the ratio of the scattering coefficient to the absorption coefficient (Sobolev 1975). In equation (2) we have assumed that the scattering process does not change the wavelength of the scattered photon (coherent scattering). The redistribution function then reduces to the scattering phase function $\Phi_\lambda(\Theta)$, where Θ is the scattering angle between the traveling direction of the incident and scattered photons, defined by

$$\cos \Theta = \mu\mu' + (1 - \mu^2)^{1/2}(1 - \mu'^2)^{1/2} \cos (\phi' - \phi) , \quad (3)$$

and ϕ is the azimuthal angle. In this paper we will use the Henyey and Greenstein (1941) scattering phase function

$$\Phi_\lambda(\Theta) = (1 - g_\lambda^2)/(1 + g_\lambda^2 - 2g_\lambda \cos \Theta)^{3/2} , \quad (4)$$

characterized by the asymmetry parameter $g_\lambda = \langle \cos \Theta \rangle$ (Wickramasinghe 1973, p. 15). In the case of isotropic scattering, $g_\lambda = 0$ and $\Phi(\Theta) = 1$.

We now write equation (1) in a dimensionless form. First, we divide equation (1) by $I_\lambda^* = \eta_\lambda^* L$, which represents the intensity emerging from a dust free ($\chi_\lambda = 0$) slab of thickness L in the direction $\mu = 1$; then we divide the resulting equation by $-\chi_\lambda$, to obtain

$$\mu\, \partial\xi_\lambda(\tau_\lambda, \mu)/\partial\tau_\lambda = \xi_\lambda(\tau_\lambda, \mu) - 1/\tau_\lambda^0 - S_\lambda(\tau_\lambda, \mu) , \quad (5)$$

where

$$\xi_\lambda(\tau_\lambda, \mu) \equiv I_\lambda(\tau_\lambda, \mu)/I_\lambda^* , \quad (6)$$

is the dimensionless intensity,

$$d\tau_\lambda = -\chi_\lambda(z)dz$$

is the differential optical depth, $\tau_\lambda^0 = \chi_\lambda L$ is the optical depth of a slab of thickness L and constant χ_λ, and

$$S_\lambda(\tau_\lambda, \mu) = (a_\lambda/4\pi) \int \xi_\lambda(\tau_\lambda, \mu')\Phi_\lambda(\Theta)d\Omega' , \quad (7)$$

is the contribution to the dimensionless source function due to scattering by dust particles. The integral in equation (7) must be carried out over all elements of solid angle $d\Omega'$ centered around the direction μ' of all incident photons which after scattering will emerge inside a solid angle $d\Omega$ around the direction μ. Since the plane-parallel slab has azimuthal symmetry, the integration over ϕ can be performed at once and the scattering source function can be written as

$$S_\lambda(\tau_\lambda, \mu) = (a_\lambda/2) \int_{-1}^{1} \xi_\lambda(\tau_\lambda, \mu')\Psi(\mu, \mu')d\mu' , \quad (8)$$

where

$$\Psi(\mu, \mu') = (1/2\pi) \int_0^{2\pi} \Phi_\lambda(\Theta)d\phi' , \quad (9)$$

is the phase function integrated over ϕ. From equation (3) it follows that $\Psi(\mu, \mu')$ obeys the following symmetry relations

$$\Psi(\mu, \mu') = \Psi(-\mu, -\mu') ,$$
$$\Psi(\mu, -\mu') = \Psi(-\mu, \mu') . \tag{10}$$

The boundary conditions for our problem are

$$\xi_\lambda(\tau_\lambda, \mu) = 0 \text{ for } \begin{cases} \tau_\lambda = 0 , & \mu < 0 , \\ \tau_\lambda = \tau_\lambda^0 , & \mu > 0 , \end{cases} \tag{11}$$

which express the fact that there is no incident radiation on the faces of the slab.

To solve equation (5) we use the method of Milkey, Shine, and Mihalas (1975). This method, adapted for the present physical situation, has been described in detail by Magris (1985) and is outlined below. For simplicity, in the remainder of this paper we will not indicate explicitly the dependence on τ_λ of the various functions, i.e., $\xi_\lambda(\mu) = \xi_\lambda(\tau_\lambda, \mu)$.

We introduce the functions $u_\lambda(\mu)$ and $v_\lambda(\mu)$, the symmetric and antisymmetric components of the dimensionless radiation field,

$$u_\lambda(\mu) \equiv [\xi_\lambda(\mu) + \xi_\lambda(-\mu)]/2 ,$$
$$v_\lambda(\mu) \equiv [\xi_\lambda(\mu) - \xi_\lambda(-\mu)]/2 , \tag{12}$$

respectively, and write the transfer equation (5) for positive and negative μ. Adding and subtracting the resulting equations we obtain

$$\mu\, du_\lambda(\mu)/d\tau_\lambda = v_\lambda(\mu) - S_\lambda^0(\mu) ,$$
$$\mu\, dv_\lambda(\mu)/dt_\lambda = u_\lambda(\mu) - S_\lambda^e(\mu) , \tag{13}$$

where

$$S_\lambda^0(\mu) \equiv [S_\lambda(\mu) - S_\lambda(-\mu)]/2 ,$$
$$S_\lambda^e(\mu) \equiv [S_\lambda(\mu) + S_\lambda(-\mu)]/2 . \tag{14}$$

Using equations (8) and (10) we can write equation (14) as

$$S_\lambda^0(\mu) = a_\lambda \int_0^1 v_\lambda(\mu')[\Psi(\mu, \mu') - \Psi(-\mu, \mu')]d\mu' ,$$
$$S_\lambda^e(\mu) = a_\lambda \int_0^1 u_\lambda(\mu')[\Psi(\mu, \mu') + \Psi(-\mu, \mu')]d\mu' + 1/\tau_\lambda^0 . \tag{15}$$

The problem is reduced to the system of two coupled first-order integro-differential equations (13), subject to the boundary conditions (eq. [11]), written in the new variables as

$$u_\lambda(\mu) = v_\lambda(\mu) \quad \text{at } \tau_\lambda = 0 ,$$
$$u_\lambda(\mu) = -v_\lambda(\mu) \quad \text{at } \tau_\lambda = \tau_\lambda^0 . \tag{16}$$

To solve equations (13) numerically, we introduce a mesh of depth points uniformly spaced in τ_λ. The derivatives in equation (13) are represented by a finite difference approximation extending over each pair of consecutive points on this mesh. The integrals over μ in equation (15) are evaluated by means of an eight-point Gaussian quadrature (Chandrasekhar 1960). A system of algebraic equations is obtained for the values of u_λ^{ij} and v_λ^{ij} at each point τ_λ^j in the mesh and in every direction μ^i used in the quadrature. The elimination scheme of Milkey, Shine, and Mihalas (1975) is used to solve this system and find u_λ^{ij} and v_λ^{ij}, which are then used to evaluate $S_\lambda^0(\mu)$ and $S_\lambda^e(\mu)$ in equation (15) by means of a Gaussian quadrature. $S_\lambda(\mu)$ and $S_\lambda(-\mu)$ are then found from equation (14). The dimensionless intensity emerging at $\tau_\lambda = 0$ is obtained from the formal solution of the transfer equation (Mihalas 1978), i.e.,

$$\xi_\lambda(\tau_\lambda = 0, \mu) = \mu^{-1} \int_0^{\tau_\lambda^0} S_\lambda(\mu) \exp(-\tau'/\mu)d\tau' ,$$
$$\xi_\lambda(\tau_\lambda = \tau_\lambda^0, -\mu) = \xi_\lambda(\tau_\lambda = 0, \mu) . \tag{17}$$

We associate a disk galaxy with a slab of material of thickness L and stellar emissivity η_λ^*, in which stars and dust grains are uniformly distributed. The radiation emerging from such a galaxy in the direction μ, expressed in magnitudes, is given according to equation (6) by

$$m_\lambda(\mu) \equiv \text{const } -2.5 \log I_\lambda(\tau_\lambda = 0, \mu) = m_\lambda^0 + C_\lambda(\mu) . \tag{18}$$

The term

$$C_\lambda(\mu) \equiv -2.5 \log \xi_\lambda(\tau_\lambda = 0, \mu) , \tag{19}$$

is computed from equation (17), and includes the correction to the galaxy magnitude due to the excess number of stellar sources along the line of sight ($\propto \mu^{-1}$) with respect to the $\mu = 1$ case, as well as the contribution due to scattering by dust grains along the direction μ. In the dust free case $C_\lambda(\mu) = 2.5 \log \mu$.

The term

$$m_\lambda^0 \equiv \text{const} - 2.5 \log (\eta_\lambda^* L) , \tag{20}$$

represents the magnitude of the dust free galaxy seen from the direction $\mu = 1$ (face on), and includes the constant defining the magnitude system.

b) *Parameters Needed to Solve the Problem*

To obtain a specific solution to equation (13) we must specify values for the following quantities appearing in the previous equations: $\eta_\lambda^* L$, a_λ, g_λ, and τ_λ^0. Without loss of generality we will assume in what follows that $\eta_\lambda^* L = 1$. For different values of this product, the value of m_λ^0 in equation (20) must be modified accordingly. The wavelength dependence of a_λ, g_λ, and τ_λ is discussed in the following section.

We experimented with the size of the mesh until we obtained values of ξ_λ that differ by less than 1%. The size of the mesh used to compute the results reported in the following sections was typically $\Delta\tau = 0.02$, and it was never larger than $\Delta\tau = 0.04$. We also tested the eight-point Gaussian quadrature. It was found to be perfectly adequate for our purpose. The uncertainties introduced by the numerical technique are smaller than those introduced by uncertainties in the values of the parameters that characterize dust grains.

c) *Optical Properties of Dust Grains*

The physical parameters that characterize the optical properties of dust grains are the albedo a_λ and the asymmetry parameter g_λ. Lillie and Witt (1976) solved the radiative transfer problem in the Galaxy and determined the values of a_λ and g_λ that reproduced the measurements of the galactic diffuse radiation obtained with the *OAO 2* satellite at $\lambda\lambda = 1550$, 1910, 2040, 2390, 2460, 2940, 2980, 3320, and 4250 Å. Morgan, Nandy, and Thompson (1976) derived a_λ at $\lambda\lambda = 2350$, and 2740 Å by fitting a theoretical model to the observations of the diffuse galactic background light obtained by the *TD-1* satellite. In this model g_λ is a free parameter. Mathis (1983) quotes the values of a_λ and g_λ at $\lambda\lambda = 3000$, 3460, 4860, 6560, 9000, 12,000, and 18,000 Å calculated by Mathis, Rumpl, and Nordsieck (1977) from a theoretical model of uncoated graphite

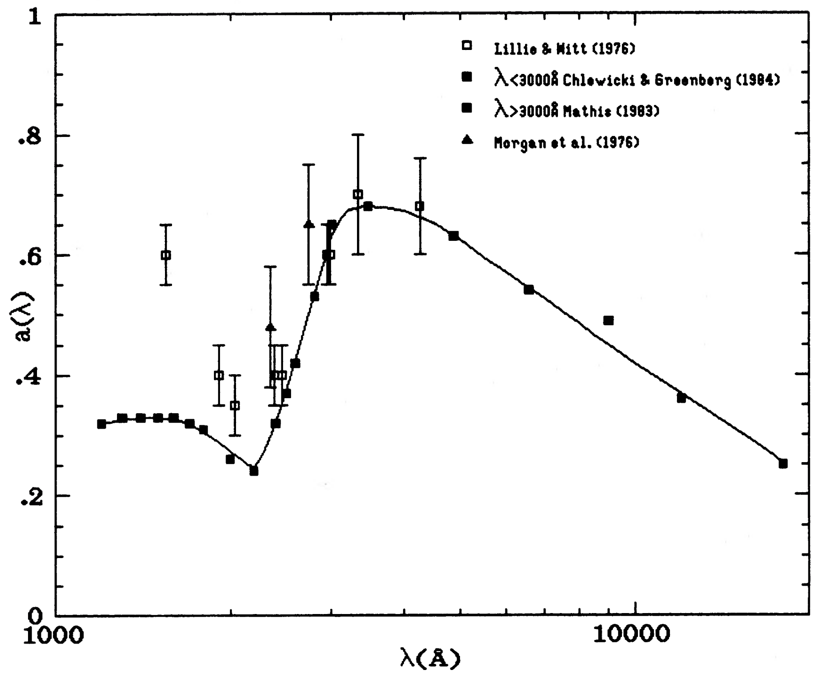

FIG. 1.—Behavior of the dust albedo, a_λ, with the logarithm of the wavelength. Data points and error bars were derived from the references listed in the figure. The smooth curve was hand-drawn by the authors. The values of a_λ on the curve are listed in Table 1 and were used in our calculations as representative values of the dust albedo.

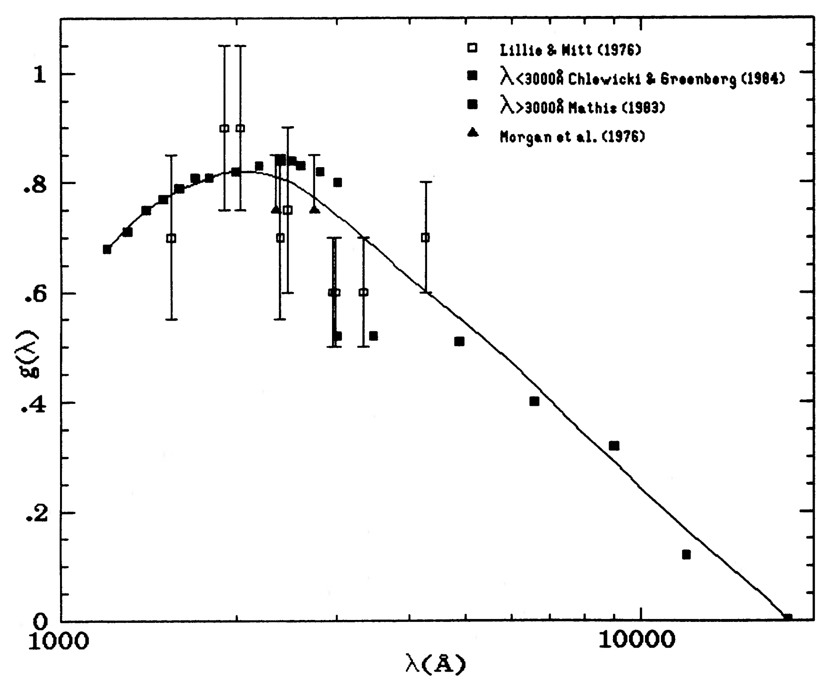

FIG. 2.—Behavior of the asymmetry parameter, g_λ, with the logarithm of the wavelength. Data points and error bars were derived from the references listed in the figure. The smooth curve was hand-drawn by the authors. The values of g_λ on the curve are listed in Table 2 and were used in our calculations as representative values of the asymmetry parameter.

1988ApJ...333..673B

and silicate particles. Chlewicki and Greenberg (1984) derive values of a_λ and g_λ for interstellar grains in the ultraviolet (from 1200 to 3000 Å) based on observations of extinction, and show that these values are more reliable than the ones determined from direct measurements of scattered light. In Figures 1 and 2 we show the different values of a_λ and g_λ, respectively. The observational points show error bars that indicate the uncertainty quoted by the authors. We use the values of a_λ derived by Morgan *et al.* for $g_\lambda = 0.75$. In the case of Chlewicki and Greenberg we use their results for model 4, corresponding to 0.018 μm silicate grains.

In order to solve the proposed problem, we need a_λ and g_λ at wavelengths at which the values of these parameters have not been determined. We drew smooth and continuous curves that approximately fit the theoretical points from Mathis (1983) and Chlewicki and Greenberg (1984). We gave more weight to the theoretical values because they form a consistent set of data. The points along these curves are listed in Tables 1 and 2, respectively, and are used as representative values of a_λ and g_λ in the calculations below. The quantities Δa_λ and Δg_λ listed in the third column of Tables 1 and 2, respectively, are a measurement of the uncertainty in the theoretical calculations; $a_\lambda \pm \Delta a_\lambda$ and $g_\lambda \pm \Delta g_\lambda$ cover the range of values obtained in the different models computed by Mathis (1983) and Chlewicki and Greenberg (1984). The high albedo reported by Lillie and Witt (1976) at 1550 Å is the only point that remains discrepant with this choice of the parameters.

d) The Extinction Law

The final quantity we need is τ_λ^0, the optical depth of the slab at a given wavelength. The optical depth τ_V^0 at the visual band V (5500 Å) is used to parametrize the results. Once a value of τ_V^0 is chosen, τ_λ^0 is computed from

$$\tau_\lambda^0 = \tau_V^0 X(\lambda)/X(V)\,, \tag{21}$$

TABLE 1

a_λ VERSUS λ

λ (Å)	$a(\lambda)$	$\Delta a(\lambda)$	$\Delta\xi_\lambda/\xi_\lambda$ $\tau_V^0 = 0.5$	$\Delta\xi_\lambda/\xi_\lambda$ $\tau_V^0 = 1$
1200.........	0.32	0.12	0.11	0.15
1300.........	0.33	0.11	0.09	0.13
1400.........	0.33	0.11	0.08	0.12
1500.........	0.33	0.10	0.07	0.11
1600.........	0.33	0.10	0.07	0.11
1700.........	0.32	0.09	0.06	0.09
1800.........	0.31	0.08	0.05	0.08
1900.........	0.29			
2000.........	0.27	0.06	0.04	0.06
2100.........	0.26			
2150.........	0.25			
2200.........	0.25	0.06	0.04	0.06
2250.........	0.26			
2300.........	0.28			
2400.........	0.32	0.08	0.05	0.08
2500.........	0.37	0.09	0.06	0.09
2600.........	0.42	0.10	0.06	0.11
2700.........	0.48			
2800.........	0.53	0.08	0.05	0.09
2900.........	0.58			
3000.........	0.63	0.15	0.11	0.19
3100.........	0.66			
3200.........	0.67			
3300.........	0.68			
3400.........	0.68			
3500.........	0.68	0.10	0.07	0.13
3600.........	0.68			
3700.........	0.68			
3800.........	0.68			
3900.........	0.67			
4000.........	0.67			
4500.........	0.65	0.10	0.06	0.11
5000.........	0.62			
5500.........	0.60			
6000.........	0.57			
6500.........	0.55	0.10	0.04	0.07
7000.........	0.53			
7500.........	0.50			
8000.........	0.49			
8500.........	0.47			
9000.........	0.45	0.10	0.03	0.05
9500.........	0.43			
10000.........	0.42			
12000.........	0.37	0.10	0.02	0.04
16500.........	0.28			
18000.........	0.25	0.10	0.01	0.02

TABLE 2

g_λ VERSUS λ

λ (Å)	$g(\lambda)$	$\Delta g(\lambda)$	$\Delta\xi_\lambda/\xi_\lambda$	$\Delta\xi_\lambda^I/\xi_\lambda^I$
1200.........	0.68	0.15	−0.02	0.02
1300.........	0.72	0.15	−0.04	0.01
1400.........	0.75	0.13	−0.04	0.00
1500.........	0.77	0.10	−0.04	0.00
1600.........	0.79	0.09	−0.04	−0.01
1700.........	0.80	0.07	−0.03	−0.02
1800.........	0.81	0.06	−0.03	−0.02
1900.........	0.82			
2000.........	0.82	0.04	−0.02	−0.02
2100.........	0.82			
2150.........	0.82			
2200.........	0.82	0.03	−0.01	−0.01
2250.........	0.82			
2300.........	0.81			
2400.........	0.81	0.04	−0.02	−0.02
2500.........	0.80	0.05	−0.03	−0.03
2600.........	0.79	0.05	−0.03	−0.03
2700.........	0.78			
2800.........	0.77	0.05	−0.03	−0.05
2900.........	0.75			
3000.........	0.74	0.05	−0.03	−0.06
3100.........	0.73			
3200.........	0.71			
3300.........	0.70			
3400.........	0.69			
3500.........	0.68	0.05	−0.02	−0.06
3600.........	0.67			
3700.........	0.66			
3800.........	0.65			
3900.........	0.64			
4000.........	0.63			
4500.........	0.58	0.05	−0.01	−0.05
5000.........	0.54			
5500.........	0.50			
6000.........	0.47			
6500.........	0.44	0.05	−0.01	−0.03
7000.........	0.40			
7500.........	0.37			
8000.........	0.34			
8500.........	0.31			
9000.........	0.29	0.05	0.00	−0.01
9500.........	0.27			
10000.........	0.24			
12000.........	0.16	0.05	0.00	0.00
16500.........	0.04			
18000.........	0.00	0.05	0.00	0.00

where $X(\lambda)$ is the extinction law. The extinction laws $X_S(\lambda)$ and $X_H(\lambda)$ given by Seaton (1979) for the Galaxy and by Howarth (1983) for the LMC, respectively, both for $R_V = 3.2$, were used in our calculations. For $\lambda > 4500$ Å, $X(\lambda)$ was obtained from Whitford (1936).

III. GENERAL RESULTS

In this section we discuss the dependence of the correction $C_\lambda(\mu)$ on the possible choices for the physical parameters that determine the solutions to equation (5).

a) Uncertainties in a_λ

As shown in Figure 1, there are large uncertainties in a_λ. To estimate the errors introduced in ξ_λ by the uncertainty Δa_λ in a_λ, we have computed ξ_λ, ξ_λ^+, and ξ_λ^-, corresponding to a_λ, $a_\lambda + \Delta a_\lambda$, and $a_\lambda - \Delta a_\lambda$, respectively. The values of the average relative error $\Delta\xi_\lambda/\xi_\lambda = (\xi_\lambda^+ - \xi_\lambda^-)/2\xi_\lambda$, listed in Table 1 as a function of λ, were computed for $\tau_V^0 = 0.5$, and 1, using $\mu = 1$, $X_S(\lambda)$, and the values of g_λ listed in Table 2. The uncertainties introduced by the albedo range from a few percent in the visible and near-IR to close to 10% in the UV. For a given a_λ, the effects of light scattering by dust grains on the radiation field increase nonlinearly with the optical depth in such a way that $\Delta\xi_\lambda/\xi_\lambda$ is an increasing function of τ_λ^0. For fixed τ_V^0 and a_λ, the uncertainties are largest for $\mu = 1$.

b) Uncertainties in g_λ

To estimate the errors introduced in ξ_λ by the uncertainties in g_λ, we computed ξ_λ, ξ_λ^+, ξ_λ^-, and ξ_λ^I, corresponding to g_λ, $g_\lambda + \Delta g_\lambda$, $g_\lambda - \Delta g_\lambda$, and $g_\lambda = 0$, respectively. The values of the average relative error $\Delta\xi_\lambda/\xi_\lambda = (\xi_\lambda^+ - \xi_\lambda^-)/2\xi_\lambda$ and the relative difference $\Delta\xi_\lambda^I/\xi_\lambda^I = (\xi_\lambda - \xi_\lambda^I)/\xi_\lambda^I$ are listed in Table 2 as a function of λ. These quantities were computed for $\tau_V^0 = 1$, using $\mu = 1$, $X_S(\lambda)$, and the values of a_λ listed in Table 1. The uncertainties introduced by g_λ are smaller at all wavelengths than the uncertainties introduced by a_λ (see col. [4] of Table 2 and col. [5] of Table 1). For fixed τ_V^0 and a_λ, $\Delta\xi_\lambda/\xi_\lambda$ and $\Delta\xi_\lambda^I/\xi_\lambda^I$ are largest for $\mu = 1$. When the optical depth increases, the probability of multiple scattering increases and, even for a non-isotropic phase function $\Phi_\lambda(\Theta)$, the radiation field becomes more isotropic, and less sensitive to g_λ.

c) Dependence on μ and τ_λ^0

In Figure 3 we plot $C_\lambda(\mu)$ versus λ for several values of μ for a fixed τ_V^0. To compute these quantities we used $X_S(\lambda)$ and the values of a_λ and g_λ listed in Tables 1 and 2. The correction C_λ is a strong function of μ for small values of τ_V^0. For larger values of τ_V^0 the slab becomes optically thick and C_λ is less sensitive to μ. Even for small values of τ_V^0, C_λ becomes independent of μ at those wavelengths at which τ_λ^0 is large, for instance at $\lambda = (1500, 2200, 4000)$ Å, where $\tau_\lambda^0 = (2.8, 3.3, 1.5)\tau_V^0$.

To study the μ dependence of the contribution of light scattering to C_λ, namely, the integral factor in equation (17), it is convenient to suppress the μ^{-1} geometrical dependence from ξ_λ. In Figure 4 we plot the function

$$G_\lambda(\mu) \equiv -2.5 \log \mu\xi_\lambda = C_\lambda(\mu) - 2.5 \log \mu \qquad (22)$$

versus λ for a given τ_V^0. The term $G_\lambda(\mu)$ becomes more positive when μ decreases because the factor $\exp(-\tau_\lambda/\mu)$ in equation (17) increases and attenuates the contribution of light scattering to the outcoming radiation. The same effect is observed when τ_V^0 increases for a fixed value of μ. For large values of τ_λ/μ, the attenuation is so pronounced that the μ^{-1} geometrical factor is compensated and C_λ becomes fainter for decreasing μ (curves cross over in Figs. 3*c* and 3*d*).

In Table 3 we list the correction term $G_\lambda(\mu)$ as a function of λ for $\mu = 0.12$, 0.26, 0.48, 0.68, 0.87, and 1, and $\tau_V^0 = 0.3$, 0.5, 1, and 2. These are the values of $G_\lambda(\mu)$ shown in Figure 4. The function $\xi_\lambda(\tau_\lambda = 0, \mu) = \mu^{-1}$ dex $[-0.4G_\lambda(\tau_\lambda, \mu)]$ can be easily derived from these tables.

As an example of the use of the results presented in this section we consider the case of a galaxy with $\tau_V^0 = 0.5$ observed at $\lambda = 5500$ Å in the direction $\mu = 0.12$. The brightening effect of the μ^{-1} factor is -2.3 mag for this μ. However, Figure 3*b* indicates that $C_v = -1.1$, i.e., the galaxy looks only 1.1 mag brighter than a dust free galaxy seen face-on. The difference of 1.2 mag is the corresponding amount of extinction when light scattering by dust grains is considered ($G_v = 1.2$ in Fig. 4*b*). This value of C_v should be compared with the value $A_V = 1.086\tau_V^0/\mu = 4.5$, obtained from a straightforward application of the cosecant law (Holmberg 1975).

Kent (1986) has found that in a band centered at 6000 Å the surface brightness profiles of spiral galaxies of a given morphological type do not depend strongly on the inclination angle. This observation is consistent with our results if the optical depth of these systems is larger than $\tau_V^0 = 1$, and maybe closer to $\tau_V^0 = 2$.

d) The Optical Depth of a Cloud

As an illustration of the use of our results, we discuss in this section the uncertainties that arise in the determination of the optical depth τ_0 of a dust cloud.

Let us consider first the case of a plane-parallel slab of non-dispersive dust ($a_\lambda = 0$) of optical depth τ_0 located *in front* of a diffuse background source of isotropic intensity I_0. The dimensionless intensity $I(\tau_0, \mu)/I_0$ of the radiation leaving this slab is, using the notation introduced in equation (6), $\xi(\tau_0, \mu) = e(\tau_0, \mu) \equiv \exp(-\tau_0/\mu)$.

Next we consider the case in which the light of the diffuse background source travels through a slab of dispersive dust. The corresponding attenuation factor $\xi(\tau_0, \mu) = E_\lambda(\tau_0, \mu)$, is obtained by solving equation (1) with $\eta_\lambda^* = 0$, and subject to the boundary conditions (written in dimensionless form)

$$\xi_\lambda(\tau, \mu) = \begin{cases} 0\,, & \text{for } \tau = 0\,, \quad \mu < 0\,, \\ 1\,, & \text{for } \tau = \tau_0\,, \quad \mu > 0\,. \end{cases} \qquad (23)$$

In Figure 5 we plot in a magnitude scale the functions $e(\tau_0, 1)$ and $E_V(\tau_0, 1)$ versus τ_0 computed for $a_\lambda = a_V = 0.60$ ($\lambda = 5500$ Å), and assuming isotropic scattering ($g_\lambda = 0$). Figure 5 shows that for a given attenuation $\xi(\tau_0, \mu)$, the value of τ_0 derived for a cloud depends on the assumptions made about the dispersive properties and the distribution of dust grains in the cloud. The lowest value of τ_0 corresponds to nondispersive dust located between the observer and the source (curve marked "e"). Dispersive dust with the same geometry gives an intermediate value of τ_0 (curve marked "E"). Dispersive dust acts as an extra source of radiation and a higher value of τ_0 is required to produce the same attenuation $\xi(\tau_0, \mu)$.

For comparison we include in Figure 5 the function $C_v(\tau_0, 1)$ defined in equation (19), which corresponds to the case of a uniform mixture of stars and dispersive dust grains with $\eta_v^* L = I_0$ (curve marked "C"). In this case, besides the dispersive dust, at any $\tau \leq \tau_0$ there are stellar sources that

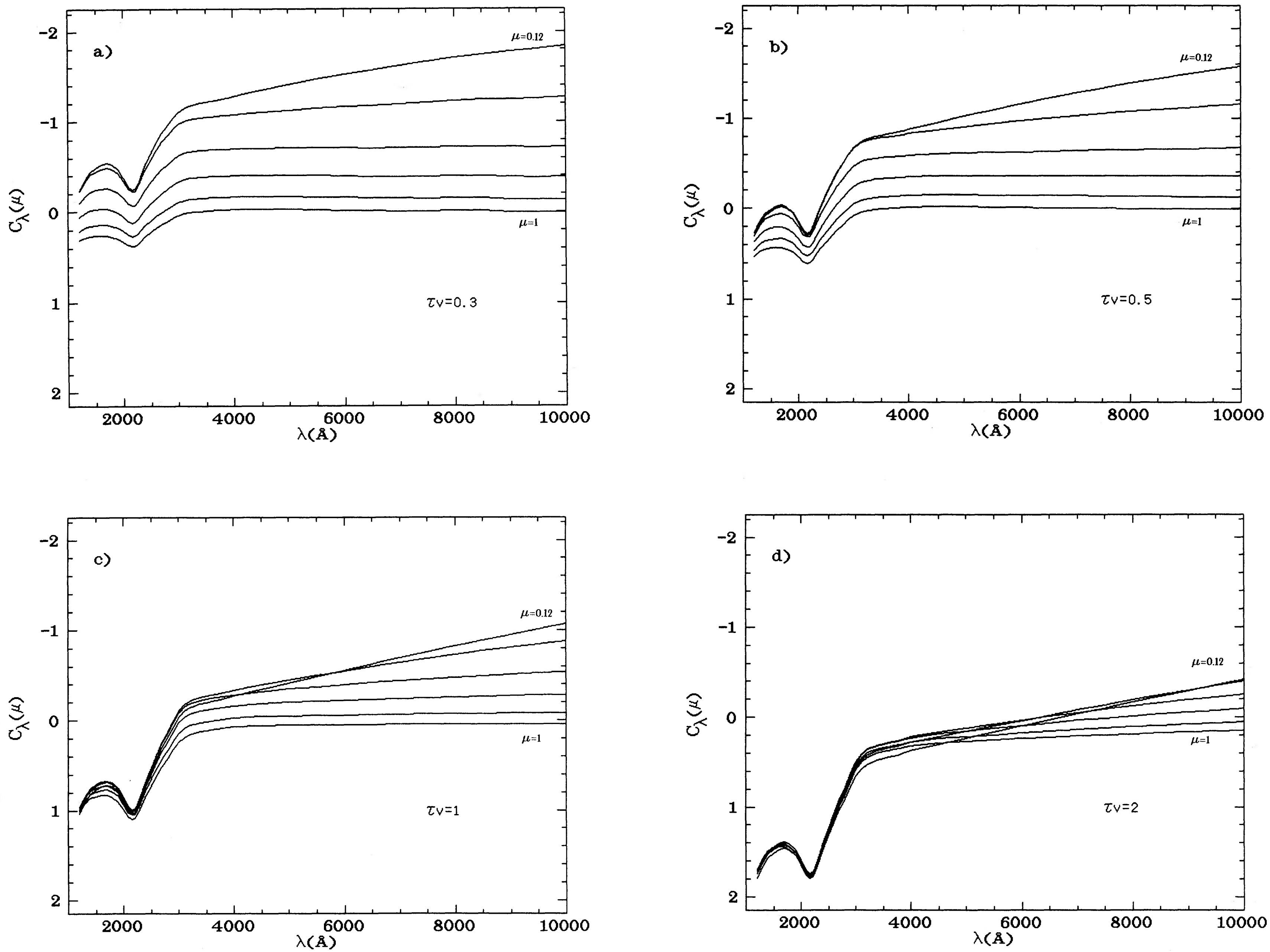

FIG. 3.—Correction C_λ in magnitudes vs. λ, for $\mu = 0.12$ (brightest), 0.26, 0.48, 0.68, 0.87, and 1 (faintest). (*a*) $\tau_V^0 = 0.3$. (*b*) $\tau_V^0 = 0.5$. (*c*) $\tau_V^0 = 1.0$. (*d*) $\tau_V^0 = 2.0$. The correction term C_λ includes the geometrical factor μ^{-1} in eq. (17). See text for details.

1988ApJ...333..673B

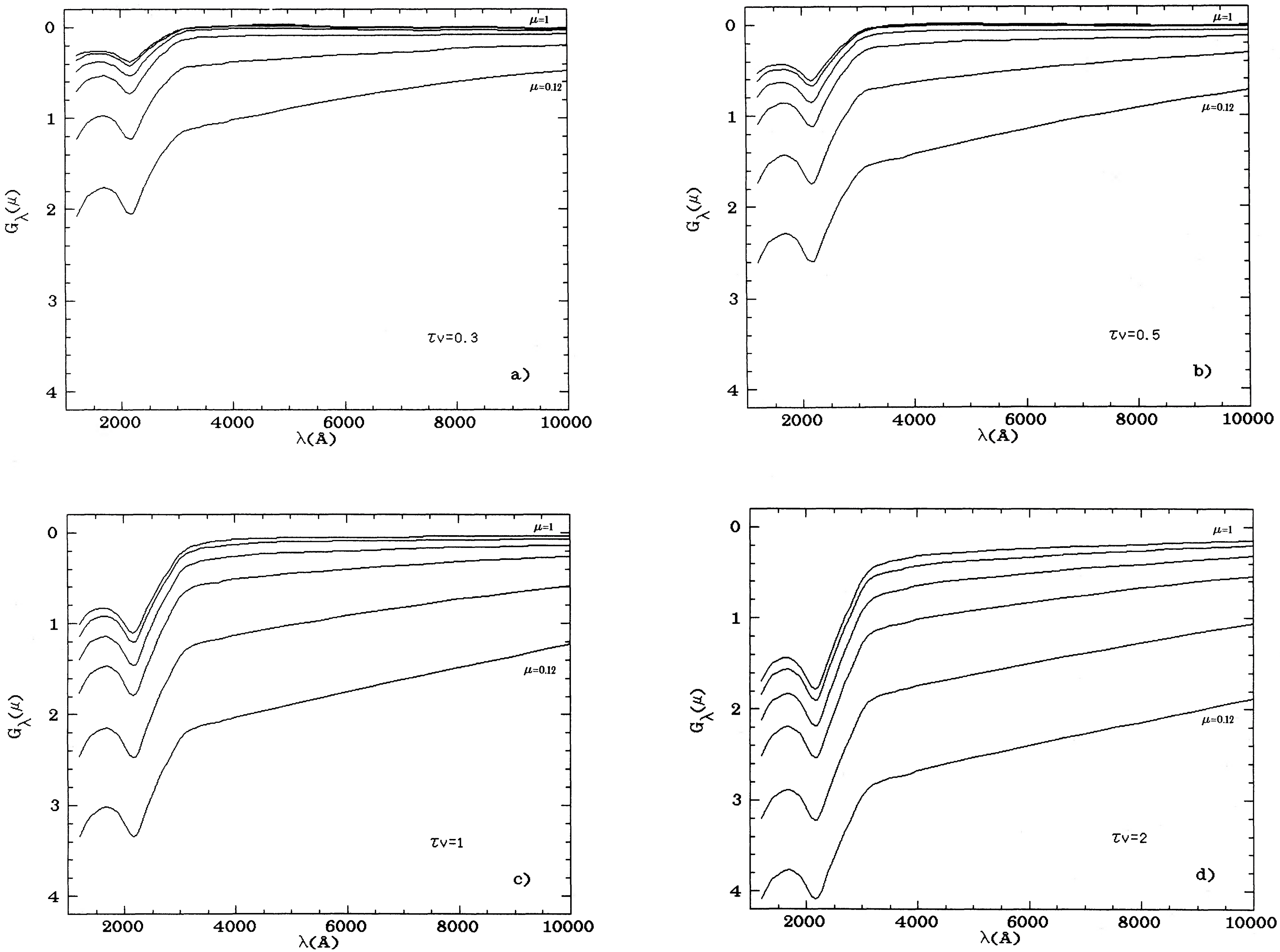

FIG. 4.—Correction G_λ in magnitudes vs. λ, for $\mu = 0.12$ (faintest), 0.26, 0.48, 0.68, 0.87, and 1 (brightest). (*a*) $\tau_V^0 = 0.3$. (*b*) $\tau_V^0 = 0.5$. (*c*) $\tau_V^0 = 1.0$. (*d*) $\tau_V^0 = 2.0$. The μ^{-1} geometrical dependence in eq. (17) has been suppressed in G_λ. See text for details.

TABLE 3

Correction $G_\lambda(\mu)$ *vs.* λ

A. $\tau_V^0 = 0.3$

	μ					
λ	0.12	0.26	0.48	0.68	0.87	1.00
1200	2.07	1.23	0.70	0.48	0.36	0.31
1300	1.95	1.13	0.63	0.43	0.33	0.28
1400	1.86	1.05	0.58	0.40	0.30	0.27
1500	1.81	1.01	0.55	0.39	0.29	0.26
1600	1.78	0.98	0.54	0.38	0.29	0.26
1700	1.76	0.97	0.53	0.38	0.29	0.26
1800	1.78	0.99	0.55	0.40	0.30	0.27
1900	1.82	1.03	0.58	0.42	0.33	0.29
2000	1.92	1.12	0.64	0.47	0.36	0.33
2100	2.03	1.21	0.71	0.52	0.40	0.36
2150	2.05	1.23	0.73	0.53	0.42	0.38
2200	2.05	1.23	0.72	0.53	0.41	0.37
2250	2.00	1.18	0.69	0.51	0.39	0.35
2300	1.93	1.12	0.64	0.47	0.36	0.33
2400	1.78	0.99	0.55	0.39	0.30	0.27
2500	1.64	0.86	0.46	0.32	0.24	0.22
2600	1.52	0.77	0.39	0.26	0.20	0.18
2700	1.42	0.68	0.32	0.21	0.15	0.14
2800	1.34	0.61	0.27	0.17	0.12	0.10
2900	1.26	0.54	0.21	0.12	0.08	0.07
3000	1.20	0.49	0.17	0.08	0.05	0.04
3100	1.15	0.45	0.14	0.06	0.02	0.02
3200	1.13	0.43	0.13	0.04	0.01	0.01
3300	1.11	0.43	0.12	0.04	0.01	0.00
3400	1.10	0.42	0.11	0.03	0.00	−0.01
3500	1.08	0.41	0.11	0.03	0.00	−0.01
3600	1.07	0.41	0.11	0.03	0.00	−0.01
3700	1.06	0.40	0.11	0.02	−0.01	−0.02
3800	1.05	0.40	0.10	0.02	−0.01	−0.02
3900	1.04	0.39	0.10	0.02	−0.01	−0.02
4000	1.02	0.38	0.10	0.01	−0.02	−0.02
4500	0.96	0.36	0.09	0.01	−0.02	−0.03
5000	0.89	0.34	0.09	0.01	−0.02	−0.03
5500	0.83	0.32	0.09	0.02	−0.01	−0.02
6000	0.78	0.30	0.09	0.02	0.00	−0.01
6500	0.73	0.29	0.09	0.03	0.00	−0.01
7000	0.68	0.27	0.09	0.03	0.00	−0.01
7500	0.64	0.26	0.09	0.04	0.01	0.00
8000	0.60	0.23	0.08	0.03	0.00	−0.01
8500	0.56	0.22	0.08	0.03	0.00	−0.01
9000	0.53	0.21	0.08	0.04	0.01	0.00
9500	0.50	0.21	0.08	0.04	0.02	0.01
10000	0.47	0.19	0.07	0.03	0.01	0.01
12000	0.36	0.14	0.06	0.03	0.01	0.00
16500	0.20	0.08	0.04	0.02	0.01	0.01
18000	0.16	0.07	0.03	0.02	0.01	0.01

TABLE 3

Correction $G_\lambda(\mu)$ *vs.* λ

B. $\tau_V^0 = 0.5$

	μ					
λ	0.12	0.26	0.48	0.68	0.87	1.00
1200	2.60	1.73	1.09	0.79	0.61	0.53
1300	2.48	1.61	0.99	0.71	0.55	0.48
1400	2.38	1.52	0.92	0.66	0.51	0.45
1500	2.34	1.48	0.89	0.64	0.49	0.44
1600	2.30	1.44	0.86	0.63	0.49	0.43
1700	2.28	1.43	0.86	0.63	0.48	0.43
1800	2.30	1.45	0.87	0.65	0.50	0.45
1900	2.35	1.50	0.92	0.69	0.53	0.48
2000	2.46	1.60	1.00	0.75	0.59	0.53
2100	2.57	1.71	1.09	0.83	0.65	0.59
2150	2.59	1.74	1.11	0.85	0.67	0.61
2200	2.59	1.73	1.11	0.84	0.67	0.60
2250	2.54	1.68	1.07	0.81	0.64	0.57
2300	2.46	1.61	1.00	0.75	0.59	0.53
2400	2.30	1.45	0.87	0.64	0.50	0.45
2500	2.15	1.30	0.75	0.54	0.41	0.37
2600	2.02	1.17	0.64	0.45	0.34	0.30
2700	1.90	1.06	0.55	0.37	0.27	0.24
2800	1.80	0.96	0.47	0.30	0.21	0.19
2900	1.71	0.87	0.39	0.24	0.16	0.13
3000	1.63	0.79	0.33	0.18	0.11	0.09
3100	1.57	0.74	0.29	0.14	0.07	0.05
3200	1.54	0.71	0.26	0.12	0.05	0.04
3300	1.52	0.70	0.25	0.11	0.04	0.03
3400	1.51	0.69	0.24	0.10	0.03	0.02
3500	1.49	0.68	0.24	0.09	0.03	0.01
3600	1.48	0.67	0.23	0.09	0.02	0.00
3700	1.47	0.66	0.23	0.08	0.02	0.00
3800	1.46	0.65	0.22	0.08	0.02	0.00
3900	1.44	0.64	0.21	0.07	0.01	−0.01
4000	1.42	0.63	0.21	0.07	0.01	−0.01
4500	1.35	0.59	0.19	0.06	0.00	−0.02
5000	1.28	0.56	0.18	0.06	0.00	−0.02
5500	1.21	0.52	0.18	0.06	0.01	−0.01
6000	1.15	0.49	0.17	0.06	0.01	−0.01
6500	1.08	0.46	0.16	0.06	0.01	−0.01
7000	1.02	0.44	0.16	0.06	0.01	0.00
7500	0.97	0.41	0.15	0.06	0.02	0.00
8000	0.91	0.39	0.15	0.06	0.02	0.00
8500	0.86	0.37	0.14	0.06	0.02	0.01
9000	0.81	0.35	0.14	0.06	0.02	0.01
9500	0.77	0.33	0.13	0.06	0.02	0.01
10000	0.72	0.31	0.12	0.06	0.02	0.01
12000	0.57	0.24	0.10	0.05	0.03	0.01
16500	0.32	0.14	0.06	0.03	0.02	0.01
18000	0.26	0.11	0.05	0.03	0.02	0.01

TABLE 3

Correction $G_\lambda(\mu)$ *vs.* λ

C. $\tau_V{}^0 = 1$

	μ					
λ	0.12	0.26	0.48	0.68	0.87	1.00
1200	3.34	2.46	1.76	1.39	1.14	1.01
1300	3.21	2.33	1.64	1.28	1.04	0.92
1400	3.12	2.24	1.55	1.20	0.97	0.87
1500	3.07	2.19	1.51	1.17	0.94	0.84
1600	3.03	2.16	1.48	1.15	0.92	0.83
1700	3.02	2.14	1.46	1.14	0.92	0.83
1800	3.04	2.17	1.49	1.17	0.94	0.86
1900	3.09	2.22	1.54	1.23	0.99	0.91
2000	3.20	2.33	1.65	1.32	1.08	0.99
2100	3.31	2.44	1.76	1.43	1.18	1.08
2150	3.34	2.47	1.79	1.45	1.20	1.10
2200	3.33	2.47	1.78	1.45	1.20	1.09
2250	3.28	2.42	1.73	1.40	1.15	1.05
2300	3.21	2.34	1.65	1.32	1.08	0.99
2400	3.04	2.16	1.48	1.16	0.94	0.85
2500	2.87	1.99	1.32	1.01	0.80	0.72
2600	2.73	1.84	1.18	0.88	0.68	0.61
2700	2.60	1.71	1.05	0.76	0.58	0.51
2800	2.49	1.59	0.93	0.65	0.48	0.42
2900	2.37	1.46	0.81	0.54	0.38	0.32
3000	2.27	1.36	0.71	0.44	0.29	0.24
3100	2.20	1.29	0.65	0.38	0.24	0.19
3200	2.16	1.25	0.61	0.35	0.21	0.15
3300	2.14	1.23	0.59	0.33	0.19	0.14
3400	2.12	1.21	0.57	0.31	0.17	0.12
3500	2.10	1.19	0.56	0.30	0.16	0.11
3600	2.09	1.18	0.55	0.29	0.16	0.10
3700	2.08	1.17	0.55	0.28	0.15	0.09
3800	2.06	1.16	0.53	0.27	0.14	0.09
3900	2.05	1.14	0.52	0.26	0.13	0.08
4000	2.03	1.13	0.51	0.26	0.13	0.07
4500	1.96	1.07	0.48	0.23	0.11	0.06
5000	1.89	1.02	0.45	0.22	0.10	0.05
5500	1.82	0.97	0.43	0.21	0.10	0.05
6000	1.75	0.91	0.40	0.20	0.09	0.05
6500	1.68	0.87	0.38	0.19	0.09	0.05
7000	1.61	0.82	0.36	0.18	0.09	0.05
7500	1.55	0.78	0.34	0.17	0.08	0.04
8000	1.48	0.73	0.32	0.16	0.08	0.04
8500	1.42	0.70	0.30	0.16	0.08	0.04
9000	1.36	0.66	0.29	0.15	0.07	0.04
9500	1.29	0.62	0.27	0.14	0.07	0.04
10000	1.23	0.59	0.26	0.14	0.07	0.04
12000	1.01	0.47	0.21	0.11	0.06	0.04
16500	0.61	0.27	0.12	0.07	0.04	0.03
18000	0.50	0.22	0.11	0.07	0.04	0.03

TABLE 3

Correction $G_\lambda(\mu)$ *vs.* λ

D. $\tau_V{}^0 = 2$

	μ					
λ	0.12	0.26	0.48	0.68	0.87	1.00
1200	4.09	3.20	2.51	2.12	1.84	1.69
1300	3.96	3.08	2.38	1.99	1.72	1.58
1400	3.87	2.98	2.29	1.91	1.63	1.50
1500	3.82	2.93	2.24	1.87	1.59	1.46
1600	3.78	2.90	2.20	1.84	1.57	1.44
1700	3.76	2.89	2.19	1.83	1.56	1.44
1800	3.79	2.91	2.22	1.86	1.59	1.47
1900	3.84	2.97	2.27	1.93	1.65	1.54
2000	3.95	3.08	2.39	2.04	1.76	1.64
2100	4.06	3.19	2.50	2.15	1.87	1.75
2150	4.09	3.22	2.53	2.18	1.90	1.78
2200	4.08	3.22	2.53	2.18	1.90	1.77
2250	4.03	3.16	2.47	2.12	1.84	1.72
2300	3.96	3.09	2.39	2.04	1.76	1.64
2400	3.78	2.91	2.21	1.86	1.58	1.47
2500	3.62	2.73	2.03	1.68	1.40	1.29
2600	3.47	2.57	1.87	1.51	1.25	1.14
2700	3.33	2.43	1.71	1.36	1.10	0.99
2800	3.21	2.29	1.57	1.21	0.96	0.86
2900	3.07	2.15	1.43	1.06	0.82	0.71
3000	2.96	2.02	1.29	0.93	0.69	0.59
3100	2.88	1.93	1.20	0.84	0.60	0.50
3200	2.83	1.89	1.16	0.79	0.55	0.45
3300	2.81	1.86	1.13	0.76	0.53	0.42
3400	2.78	1.84	1.11	0.74	0.51	0.40
3500	2.76	1.82	1.09	0.72	0.49	0.38
3600	2.75	1.81	1.08	0.71	0.48	0.37
3700	2.74	1.79	1.07	0.69	0.47	0.36
3800	2.72	1.78	1.05	0.68	0.45	0.34
3900	2.70	1.76	1.03	0.66	0.44	0.33
4000	2.68	1.74	1.02	0.65	0.43	0.32
4500	2.60	1.68	0.96	0.60	0.39	0.29
5000	2.53	1.62	0.92	0.57	0.37	0.27
5500	2.47	1.56	0.88	0.54	0.35	0.25
6000	2.40	1.50	0.83	0.51	0.33	0.24
6500	2.33	1.44	0.79	0.48	0.31	0.22
7000	2.27	1.38	0.75	0.45	0.29	0.21
7500	2.20	1.33	0.71	0.43	0.27	0.20
8000	2.14	1.27	0.67	0.41	0.26	0.19
8500	2.07	1.22	0.64	0.39	0.24	0.18
9000	2.01	1.16	0.60	0.36	0.23	0.17
9500	1.94	1.11	0.57	0.34	0.22	0.16
10000	1.88	1.06	0.54	0.32	0.20	0.15
12000	1.62	0.86	0.43	0.26	0.16	0.12
16500	1.07	0.52	0.25	0.15	0.10	0.07
18000	0.90	0.43	0.21	0.13	0.09	0.07

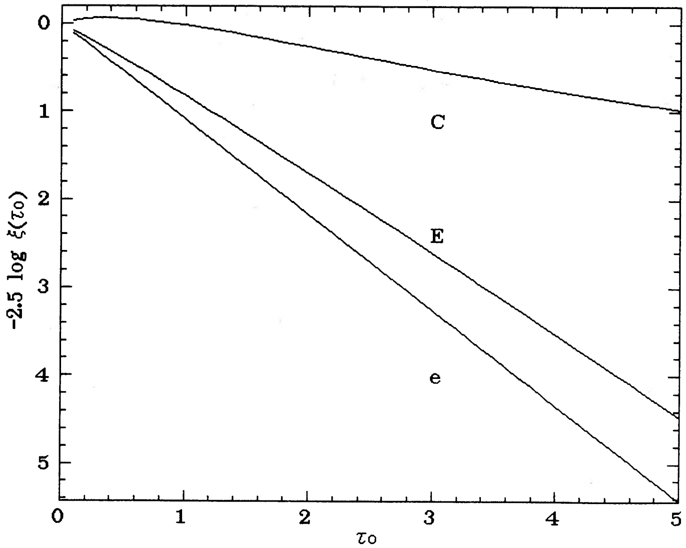

FIG. 5

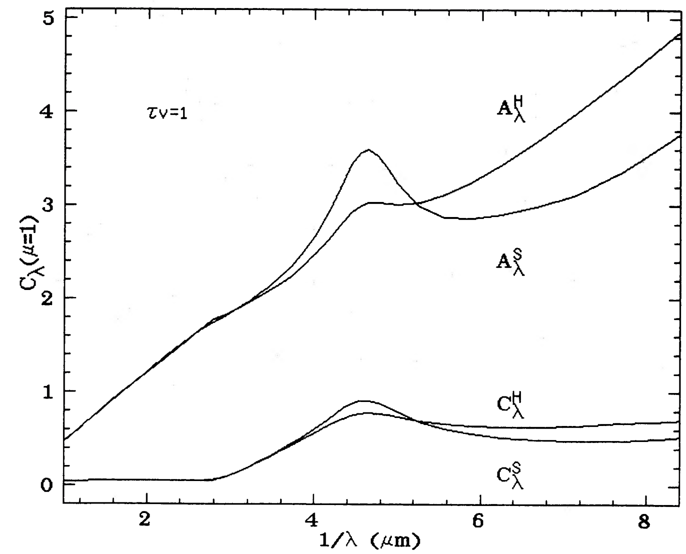

FIG. 6

FIG. 5.—Behavior of the different attenuation terms with τ_0 for $\mu = 1$. The curve marked "e" corresponds to nondispersive dust located between an observer and a diffuse background source. The curve marked "E" corresponds to the same geometry but for dispersive dust. The curve marked "C" corresponds to a uniform mixture of stars and dispersive dust. For a given $\xi(\tau_0)$, curve e gives the minimum value of τ_0. Curve C gives the maximum value. See text for details.

FIG. 6.—Comparison of the extinction curves $A^S_\lambda = 1.086X_S(\lambda)$ and $A^H_\lambda = 1.086X_H(\lambda)$ with the correction terms C^S_λ and C^H_λ, computed using $X_S(\lambda)$ and $X_H(\lambda)$ in eq. (21), respectively. All curves were computed for $\tau^0_V = 1$. The correction terms are shown for $\mu = 1$.

contribute to the intensity leaving the slab and a much larger τ_0 is required to obtain the same attenuation factor $\xi(\tau_0, \mu)$ than with curves e or E. The choice $\eta^*_v L = I_0$ is arbitrary, but it is included here for illustration purposes.

We conclude that, if scattering occurs and is neglected, the optical depth τ_0 of the cloud is underestimated by using the exponential factor, $\xi_\lambda(\tau_0, \mu) = \exp(-\tau_0/\mu)$. Similarly, the intensity $\xi_\lambda(\tau_0, \mu)$ leaving the cloud for a given τ_0, is underestimated if we use $\exp(-\tau_0/\mu)$ as the attenuation factor, instead of $E_\lambda(\tau_0, \mu)$ or $C_\lambda(\tau_0, \mu)$.

e) Comparison with the Extinction Curve

In this section we discuss the dependence of the correction term C_λ on the extinction curve $X(\lambda)$ used in equation (21). In Figure 6 we compare the extinction curves, $A^S_\lambda = 1.086X_S(\lambda)$ and $A^H_\lambda = 1.086X_H(\lambda)$, with the correction terms C^S_λ and C^H_λ, computed using $X_S(\lambda)$ and $X_H(\lambda)$ in equation (21), respectively. All curves were computed for $\tau^0_V = 1$. The correction terms are shown for $\mu = 1$.

The runs of a_λ and g_λ with λ discussed in § II were derived assuming dust particles with the properties of the galactic dust. The use of these values of a_λ and g_λ with $X_H(\lambda)$, the extinction law for the LMC, is not strictly correct, and it is justified only as a test of the sensitivity of our results to the shape of $X(\lambda)$.

The shape of the curve C_λ follows the behavior of the extinction curve $X(\lambda)$ used to compute it. In Figure 6 it is apparent that the 2200 Å feature is shallower in the curves A^H_λ and C^H_λ than in the curves A^S_λ and C^S_λ. Similarly, for $\lambda < 1900$ Å the curves A^H_λ and A^S_λ show the same relative behavior as the curves C^H_λ and C^S_λ.

The extinction derived from the curves A_λ in Figure 6 is larger than that derived from the curves C_λ. As discussed in § III*d*, the standard extinction correction, A_λ, includes only absorption processes, while the correction C_λ takes into account the scattering of photons into the line of sight by dust particles. The scattering process amounts to an extra source of radiation that reduces the extinction produced by a dust cloud of a given τ^0_V. In the visible region the difference $A_\lambda - C_\lambda$ is close to 1 mag, whereas it reaches over 3 mag in the UV. The effects of scattering are more significant for large optical depths. In the visible and the IR the difference between both sets of curves decreases because τ_λ is smaller at these λ than in the UV. For $\lambda > 3600$ Å, the values of τ^0_λ and a_λ are such that the corrections C_λ are close to zero, indicating that for these λ's as many photons are scattered into the line of sight as are absorbed from the beam ($\xi_\lambda \approx 1$). This behavior is also seen in Figure 3*c*.

f) Stratified Mixture of Stars and Dust

We assume a slab of thickness δ, where stars and dust grains are distributed homogeneously, surrounded on both sides by slabs of thickness D containing stars only. For simplicity we assume that the stellar emissivity, $\eta^*_\lambda(z, \mu)$, is the same in the three slabs and that the scattering process is isotropic ($g_\lambda = 0$). This is a crude approximation since, in reality, the density of stars and the distribution of spectral types are functions of z. However, we think the model is good enough for our purpose of testing the sensitivity of the correction term C_λ to the assumption of a uniform distribution of stars and dust grains.

In Figure 7 we show the correction term C_λ versus λ for several values of the ratio $\beta \equiv \delta/D$, inclination $\mu = 1$, and $\tau^0_V = 0.5$, and 1. In this case τ^0_V is the optical depth of the central slab. The total thickness of the system $L = (\beta + 2)D$ is the same in all cases. The extreme case, $\beta = 100$, is equivalent to the uniform slab discussed before and is included for comparison with our previous results.

For $\tau^0_V = 0.5$, the dust in the inner layer attenuates the radiation leaving the dust-free background layer and C_λ is larger (fainter) than in the uniform galaxy ($\beta = 100$). As β increases, light scattering by dust grains occurs in a larger fraction of the galaxy. The probability that photons are scattered into the line of sight increases, and C_λ becomes smaller (brighter).

For larger optical depths ($\tau_V^0 = 1$), the radiation leaving the stratified galaxy is produced mainly in the dust-free foreground layer. As β increases, this layer becomes less significant and C_λ becomes more positive (fainter). The uniform mixture, $\beta = 100$, is the faintest because in this case the light produced over the whole galaxy is attenuated by dust.

The cross over of the C_λ curves in Figure 7 is due to the change from the small to the large optical depth regime, according to the run of $X(\lambda)$ with wavelength.

The differences in C_λ for the stratified and the uniform cases are at most a few tenths of a magnitude (in the UV for $\tau_V^0 = 1$). These differences are of the same order of magnitude as the uncertainties due to a_λ and g_λ discussed in § III*a*, *b*. In view of these results, we conclude that our assumption of a uniform mixture of stars and dust grains seems justified.

IV. APPLICATIONS

a) The Dependence of the Extinction on the Cosmological Redshift

The intensity of the radiation leaving a dust-free plane-parallel galaxy of thickness L, in the μ direction, is given by $\eta_\lambda^* L\mu^{-1}$, where η_λ^* is the stellar emissivity. Let $m_{\lambda_0}(Z, \mu)$ be the

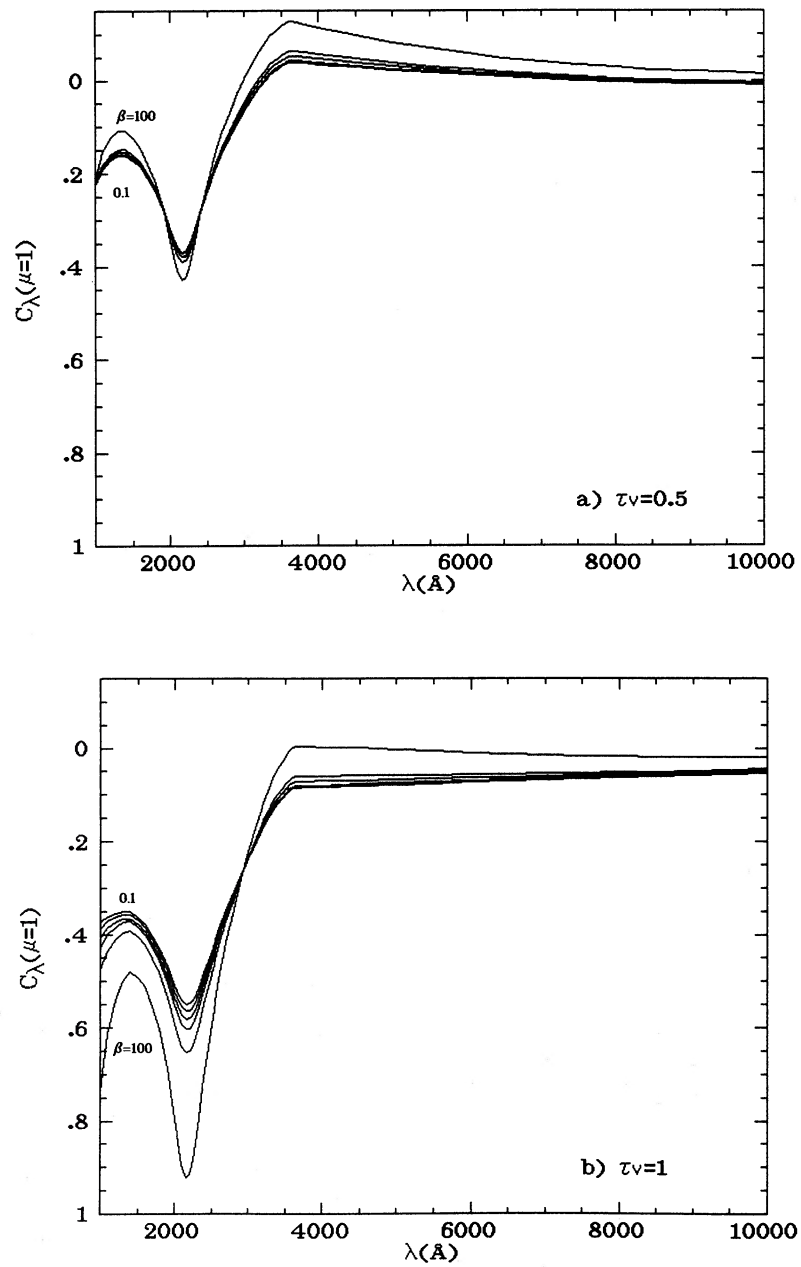

FIG. 7.—Correction term C_λ vs. λ for a stratified galaxy for $\mu = 1$, and $\beta \equiv \delta/D = 0.1, 0.2, 0.3, 0.5, 1$, and 100. (*a*) $\tau_V^0 = 0.5$. (*b*) $\tau_V^0 = 1$. See text for details.

corresponding observer's frame magnitude of the galaxy when seen at redshift Z through a filter of effective wavelength λ_0.

The intensity of the radiation leaving a system in which the same stellar population is mixed with dust grains is, according to equation (22), $\eta_\lambda^* L \xi_\lambda(\tau_\lambda = 0,\ \mu) = \eta_\lambda^* L \mu^{-1}$ dex $[-0.4 G_\lambda(\tau_\lambda, \mu)]$. Let $m_{\lambda_0}(Z, \tau_\lambda, \mu)$ be the corresponding magnitude in the observer's rest frame.

The difference between the observer's frame magnitude of the dusty and the dust-free galaxies, seen at the same redshift and with the same inclination, is

$$\Delta m_{\lambda_0}(Z) \equiv m_{\lambda_0}(Z, \tau_\lambda, \mu) - m_{\lambda_0}(Z, \mu)\ . \qquad (24)$$

The difference $\Delta m_{\lambda_0}(Z)$ is due to the attenuation of light in the dusty galaxy, and depends on μ only through the term $G_\lambda(\tau_\lambda, \mu)$, since the factors μ^{-1} appearing in m_{λ_0} cancel out.

The quantity $\Delta m_{\lambda_0}(Z)$ has been computed for the *UBV* system, as well as for the two HST filters B220 and B275, following the procedures and the filter response functions given by Bruzual (1981). The last two filters have effective wavelengths 2200 and 2750 Å, respectively. The magnitudes through these filters will be denoted "22" and "27," respectively, as in Bruzual (1981).

In Figure 8 we show the behavior with Z of $\Delta m_{\lambda_0}(Z)$ in the observer's frame for several values of μ in the 22, 27, U, B, and

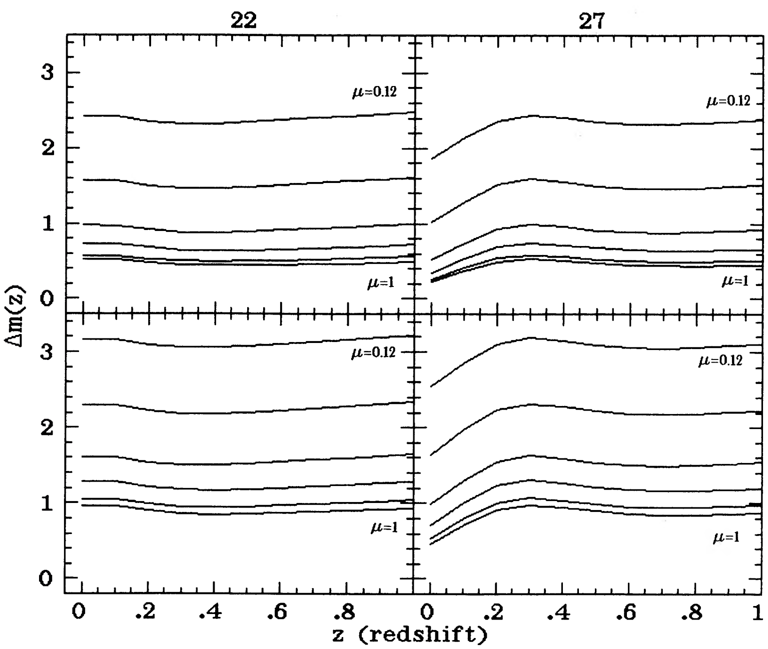

FIG. 8*a*

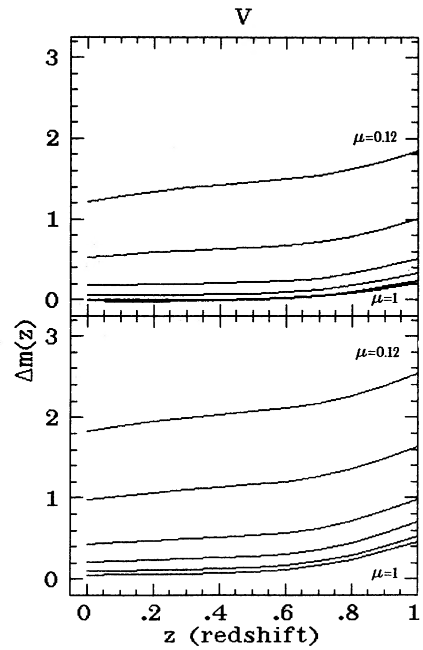

FIG. 8*c*

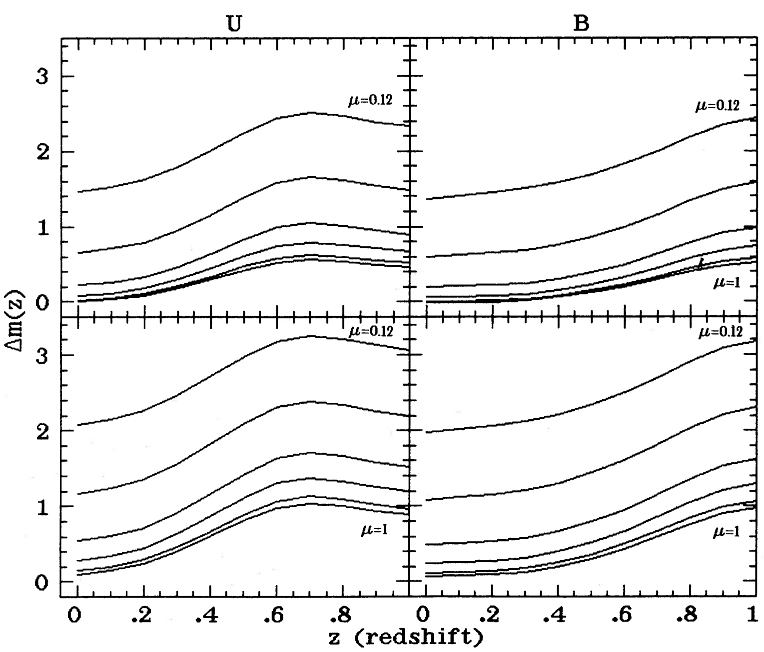

FIG. 8*b*

FIG. 8.—Behavior of $\Delta m_{\lambda_0}(Z)$ with Z in the observer's frame for $\mu = 0.12$ (*top*), 0.26, 0.48, 0.68, 0.87, and 1 (*bottom*). The top frame corresponds to $\tau_V^0 = 0.5$; the bottom one to $\tau_V^0 = 1.0$. (*a*) 22 and 27 bands. (*b*) U and B bands. (*c*) V band.

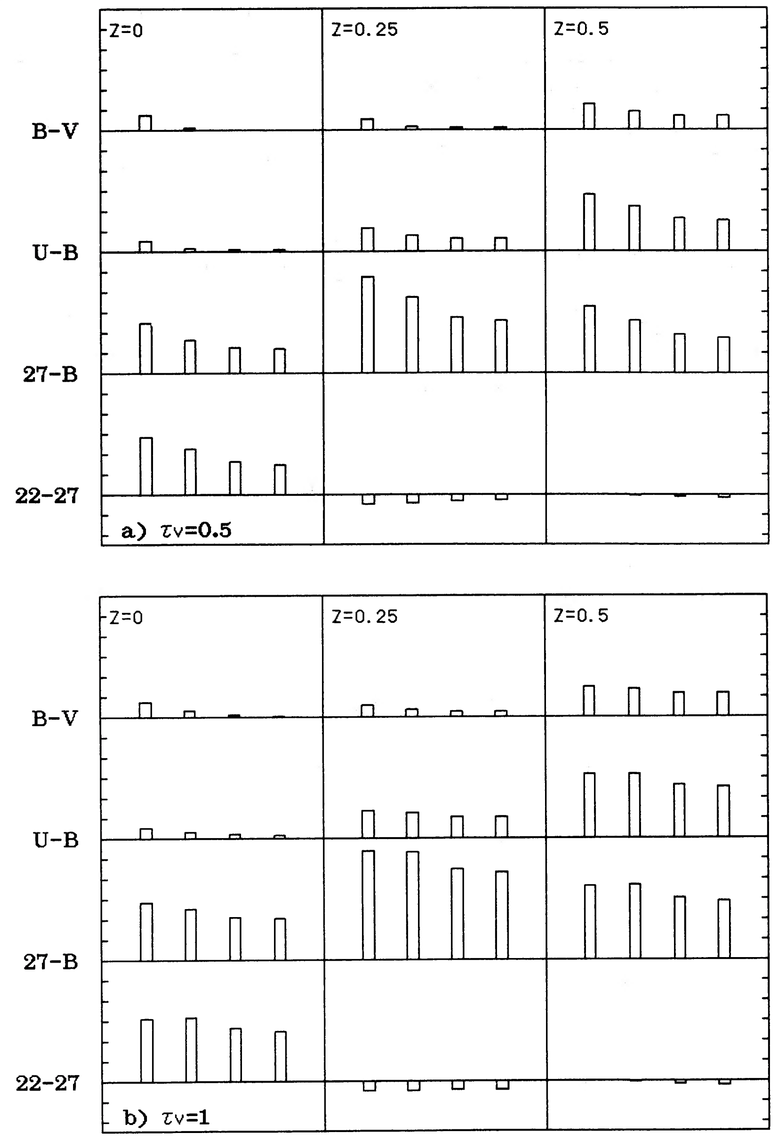

FIG. 9.—Color difference between a dusty and a dust-free galaxy, seen with the same inclination at redshift Z in the observer's frame. The differences are shown for the colors $22-27$, $27-B$, $U-B$, and $B-V$, for $Z = 0$, 0.25, and 0.5. The bars on each frame represent the color difference for $\mu = 0.12$ (*left*), 0.48, 0.87, and 1 (*right*). The height of each frame is 1.2 mag. The horizontal spacing is arbitrary. (*a*) $\tau_V^0 = 0.5$. (*b*) $\tau_V^0 = 1$.

V bands. Two frames are shown for each band. The top frame corresponds to $\tau_V^0 = 0.5$; the bottom one to $\tau_V^0 = 1.0$. The correction terms $G_\lambda(\mu)$ do not change by a large amount over the wavelength range covered by a typical filter, and $\Delta m_{\lambda_0}(Z)$ is practically independent of η_λ^*. In order to compute $\Delta m_{\lambda_0}(Z)$, we used Kurucz (1979) model SED for an A0 V star as a representative η_λ^* for a disk galaxy. The quantities shown in the figure can be used with different SEDs.

For a given τ_V^0, the difference $\Delta m_{\lambda_0}(Z)$ increases when μ decreases due to the larger effective optical depth along the line of sight. For a fixed μ, $\Delta m_{\lambda_0}(Z)$ increases with τ_V^0. A galaxy may look up to 3 mag fainter (depending on μ) than a similar galaxy with no dust and the same inclination. The bands with shorter λ_0 show a higher amount of extinction for low Z.

b) Reddening and Cosmological Redshift

We now compute the difference in color in the observer's frame, analogous to equation (24), between the dusty and the dust-free galaxy, seen with the same inclination at redshift Z. In Figure 9 we show these differences for the colors $22-27$, $27-B$, $U-B$, and $B-V$, for $Z = 0$, 0.25, and 0.5. The bars on each frame represent the color difference for $\mu = 0.12$ (*left*), 0.48, 0.87, and 1 (*right*). The height of each frame is 1.2 mag. The horizontal spacing is arbitrary. To compute the color differences we used again Kurucz (1979) model SED for an A0 V star as a representative η_λ^* for a disk galaxy. As in the previous section, the color differences are practically independent of η_λ^*. The quantities shown in Figure 9 can be used with different SEDs.

The differences in color in the observer's frame are larger for $\tau_V^0 = 1$ than for $\tau_V^0 = 0.5$. In general, the lower values of μ show the larger color differences. The differences in $27-B$ at $Z = 0.25$ reach almost 1 mag for low values of μ. At $Z = 0$ and 0.25, both galaxies have almost the same $B-V$ color for large μ. As Z increases, the U and B bands sample the UV spectral region, where the effects of extinction are larger, and the color differences in $U-B$ and $B-V$ increase. At $Z = 0.25$ and 0.5 the dusty galaxy looks bluer in $22-27$ than the dust-free galaxy. This happens because the contribution of scattering to the light leaving the galaxy at the rest frame wavelengths 1760 and 880 Å, sampled by the 22 band at these values of Z, is larger than at the rest frame wavelengths 2160 and 180 Å, sampled by the 27 band.

c) *Comparison with the Cosecant Law*

The magnitude and color differences computed with the standard extinction curve $X_S(\lambda)$ and the cosecant law are larger than the ones shown in Figures 8 and 9. For instance, the cosecant law in the case $\tau_V^0 = 0.5$, $\mu = 0.48$, gives $\Delta m = (3.7, 2.4, 1.8, 1.5, 1.1)$ for the (22, 27, U, B, V) bands at $Z = 0$, respectively. The corresponding values for $Z = 0.25$ are $\Delta m = (3, 3.8, 2.2, 1.9, 1.5)$, and for $Z = 0.5$, $\Delta m = (3.2, 3, 3.1, 2.2, 1.8)$. These values of Δm are between 1 and 2 mag larger than the ones shown in Figure 8. As shown in § III, the attenuation of light is over estimated when scattering is neglected.

Similarly, the color differences predicted with the cosecant law are larger than the ones shown in Figure 9. In the same case considered above, $\tau_V^0 = 0.5$, $\mu = 0.48$, the color differences derived from the cosecant law are $\Delta(22-27, 27-B, U-B, B-V) = (1.3, 0.9, 0.3, 0.4)$ at $Z = 0$. The corresponding values for $Z = 0.25$ are $(-0.8, 1.9, 0.3, 0.4)$, and for $Z = 0.5$ $(0.2, 0.8, 0.9, 0.4)$.

In consequence, the standard extinction curve, $X_S(\lambda)$, used in conjunction with the cosecant law, predicts dusty galaxies to be redder and fainter than the solution of the radiative transfer equation including light scattering by dust grains discussed in this paper.

V. SUMMARY AND CONCLUSIONS

We have approximated a disk galaxy by an infinite plane-parallel homogeneous distribution of stars and dispersive dust grains, with the same optical properties as galactic dust. The intensity of the radiation emerging from such a galaxy in the direction μ is given by equation (17). This solution shows the expected μ^{-1} dependence on the inclination to the line of sight. This geometrical factor is due to the excess number of stellar sources along the line of sight with respect to the $\mu = 1$ case. The integral factor in equation (17) represents the contribution to the emerging intensity from stellar light scattered by dispersive dust grains.

The correction terms $C_\lambda(\mu)$ and $G_\lambda(\mu)$ are uncertain due to the poorly known quantities a_λ and g_λ that describe the optical properties of dust grains. To simplify our calculations we neglected the stratification in the distribution of stars and dust grains existing in disk galaxies. However, these uncertainties and assumptions do not affect the main conclusions of this paper. Relaxing the assumption of a nonstratified uniform mixture of stars and dust grains, did not change our correction terms by more than 1/10 or 2/10 of a magnitude. These changes are smaller than the uncertainties introduced by a_λ and g_λ. Since galaxies are not infinite planes, there is a lower limit to the inclination μ for which our results have a physical meaning. The lowest value we used, $\mu = 0.12$, is well above this limit.

The effects of the cloudy nature of the distribution of dust in galaxies have not been evaluated in this paper. The reader should keep in mind that our correction terms apply only to systems in which dust has identical properties to the galactic dust, is distributed with plane-parallel symmetry, and is uniformly mixed with stars.

The correction terms $G_\lambda(\mu)$ give the attenuation of stellar light due to the presence of dispersive dust in a galaxy. The resultant effects of dispersive dust on the light leaving the galaxy at a given wavelength depend on the dust optical depth at that wavelength. The attenuation suffered by the light emitted by diverse sources in the galaxy is less than the exponential attenuation produced by nondispersive dust with the same optical depth placed in front of the sources. Light scattering acts as an extra source of radiation, since photons are not only removed but added to the light beam. In contrast, in the pure absorption case, photons are only removed from the beam.

The correction terms $G_\lambda(\mu)$ listed in Table 3 should be used as indicated in § IV to predict magnitudes and colors of galaxies as a function of redshift, as well as to obtain intrinsic magnitudes and colors from the observed values. The use of the standard extinction curve and the cosecant law produces magnitudes of dusty galaxies that are fainter by as much as 2 mag than the ones obtained from the quantity Δm shown in Figure 8. Similarly, the colors of dusty galaxies derived from the cosecant law differ by up to 1 mag from the colors predicted according to our calculations. We conclude that our correction terms should be preferred over the standard cosecant law to derive the photometric properties of dusty galaxies.

Kent (1986) has shown that surface brightness profiles of spiral galaxies do not depend strongly on the inclination μ. This fact suggest that these galaxies are optically thick, and that one should use our results for $\tau_V^0 > 1$.

The ideas for this paper originated from discussions between one of us (G. B. A.) and P. Jakobsen. This research has been supported in part by the Consejo Nacional de Investigaciones Cientificas y Tecnológicas (CONICIT) under projects S1-1615 and F-58. We received ample support in the use of the computing facilities of the Centro Cientifico IBM in Caracas. Part of this paper was submitted by G. M. C. as a Senior Physics thesis to the Universidad Simón Bolívar in Caracas.

REFERENCES

Bruzual A., G. 1981, Ph.D. thesis, University of California, Berkeley.
———. 1983, *Ap. J.*, **273**, 105.
Bruzual A., G., and Kron, R. 1980, *Ap. J.*, **241**, 25.
Chandrasekhar, S. 1960, *Radiative Transfer* (New York: Dover).
Chlewicki, G., and Greenberg, J. M. 1984, *M.N.R.A.S.*, **211**, 719.
Elmegreen, D. M. 1980, *Ap. J. Suppl.*, **43**, 37.
Henyey, L. G., and Greenstein, J. L. 1941, *Ap. J.*, **93**, 70.
Holmberg, E. 1975, in *Stars and Stellar Systems*, Vol. **9**, *Galaxies and the Universe*, ed. A. Sandage, M. Sandage, and J. Kristian (Chicago: University of Chicago Press), p. 123.
Howarth, I. D. 1983, *M.N.R.A.S.*, **203**, 301.
Kent, S. 1986, *A.J.*, **91**, 6.
Koo, D. 1981, Ph.D. thesis, University of California, Berkeley.
Kurucz, R. 1979, *Ap. J. Suppl.*, **40**, 1.
Lillie, C. F., and Witt, A. N. 1976, *Ap. J.*, **208**, 64.
Magris, C. G. 1985, Senior Physics Thesis, Universidad Simón Bolívar and CIDA, Venezuela.
Mathis, J. S. 1983, *Ap. J.*, **267**, 119.
Mathis, J. S., Rumpl, W., and Nordsieck, K. H. 1977, *Ap. J.*, **217**, 425.
Mihalas, D. 1978, *Stellar Atmospheres* (San Francisco: Freeman).
Milkey, R. W., Shine, R. A., and Mihalas, D. 1975, *Ap. J.*, **202**, 250.
Morgan, D. H., Nandy, K., and Thompson, G. I. 1976, *M.N.R.A.S.*, **177**, 531.
Roberge, W. G. 1983, *Ap. J.*, **275**, 292.
Sadler, E. M., and Gerhard, O. E. 1985, *M.N.R.A.S.*, **214**, 177.

Seaton, M. J. 1979, *M.N.R.A.S.*, **187**, 73p.
Sobolev, V. 1975, *Light Scattering in Planetary Atmospheres* (Oxford: Pergamon).
Tinsley, B. M. 1980, *Ap. J.*, **241**, 41.
Whitford, A. E. 1936, *Ap. J.*, **83**, 424.
Wickramasinghe, N. C. 1973, *Light Scattering Functions for Small Particles* (London: Hilger), p. 15.

GUSTAVO BRUZUAL A., GLADIS MAGRIS C., and NURIA CALVET: Centro de Investigaciones de Astronomia, Apartado Postal 264, Mérida 5101-A, Venezuela